Optical emissions in a sonoluminescing bubble

T. W. Chen, P. T. Leung, and M.-C. Chu
Department of Physics, The Chinese University of Hong Kong, Hong Kong, China
(Received 14 March 2000)

We study how the mechanism of spontaneous decay of atoms (or molecules) in a sonoluminescing bubble (SLB) can be affected by the high density and high temperature environment resulting from the rapid collapse of the gas bubble immediately prior to light emission. We present a detailed study of the density of states of photons in multiple-layered spheres, which mimic various stages of a SLB. In particular, we found that the spontaneous decay rate could be strongly enhanced in the presence of a thin plasma shell inside the bubble, which was predicted recently in numerical hydrodynamic simulations of a SLB.

PACS number(s): 78.60.Mq, 42.50.Ct, 42.50.−p, 47.55.Dz

I. INTRODUCTION

Sonoluminescence (SL) is the phenomenon by which a gas bubble in water (or other liquids) is driven to oscillate and glow by external acoustic waves. This phenomenon has been known for over half a century [1,2]; however, there has been a revival of interest in the subject since direct experimental observations of stable single bubble sonoluminescence (SBSL) became possible in the early 1990s [2–7]. The conversion of sound into light energy in SL represents a 10^{12}-fold concentration of energy [2], which bears obvious implications on possible technological applications in chemistry and materials science [8]. Many remarkable and intriguing physical phenomena (or models) related to SBSL have been proposed, such as shock wave formation [9–15], rectifying diffusion [16], nuclear fusion [10,11], and proton tunneling [17].

In a SL experiment [2,5,18–26], a gas bubble is trapped at the antinode of a standing ultrasound wave of frequency around 25 kHz in a partially degassed liquid, typically water. Under a proper driving pressure, ranging from 1.15 to 1.5 atm, the bubble grows to a maximum size of about 50 μm in radius, and then collapses rapidly to a minimum size of about 0.5 μm in radius, at which a flash of light with an intensity of the order 1–10 mW (a total energy of 10^5–10^6 eV) could be observed [2]. The pulse width of the flash measured ranges from 40 to 350 ps [27]. This is even shorter than the typical time scale of the spontaneous decay of atoms (or molecules) in free space, and is one of the most salient features of SBSL. The spectrum observed resembles that of black-body radiations. It is continuous and does not exhibit any line (or band) structure, regardless of the types of gas used in the experiments [2,20]. It also shows a near-exponential falloff with increasing wavelengths (to 800 nm), and a broad maximum at short wavelengths.

The time dependence of the bubble radius has been measured using light scattering techniques with a resolution of less than 10 ns [5,18,19,25]. For a bubble initially doped with 1% of argon, it was observed that at about 10 ns before the bubble attained its minimum radius and prior to the emission of the flash, the bubble collapsed with a speed more than four times the ambient speed of sound in the gas [26]. As a consequence of the rapid collapse, shock waves may develop inside the bubble, as predicted in some numerical simulations [9–13]. Various models based on shock wave related mechanisms have been proposed to explain SL [9–15]. For example, recent numerical simulations showed that a thin plasma shell is likely to develop during the formation of shock waves [15]. However, it is also generally believed that regions of high density and high temperature exist during the collapsing phase of a sonoluminescing bubble (SLB), even in the absence of shock waves [12,13].

A natural attempt to account for the SL flash is based on blackbody radiation. By matching the spectra obtained in experiments with the theoretical spectrum of a blackbody, the temperatures of the glowing gas are estimated to be of the order 10^4–10^5 K [2,20]. Such a high temperature could be achievable when a SLB collapses to its minimum size [12,13]. In fact, a SL model incorporating the blackbody radiation emission mechanism and photon-absorption process was recently proposed, and it nicely reproduced the observed parameter dependences of the pulse width and the spectrum of the light pulses [28].

However, it usually takes several nanoseconds for excited atoms (or molecules) to decay via the spontaneous emission of radiation. The lifetime is too long compared with the observed SL pulse widths. Hence other, more sophisticated, deexcitation processes, such as radiative recombination, radiative electronic transitions, radiative rotational or vibrational transitions, bremsstrahlung, or even collision-induced emission, have been invoked [29]. Electron-ion bremsstrahlung is probably the most promising among these mechanisms, yet it is still far from definitive [29]. On the other hand, there have been several studies that relate SL to the generation of photons by the motion of the bubble wall separating the two phases (water and gas) in a SLB [30]. However, the power derived from this model is much smaller than the experimentally observed values in SL [2].

In order to understand the emission mechanism of SBSL, we propose to study how the mechanism of optical emission could be affected by the unusual environment developed in a SLB. There are several important physical factors that are worthy of remark. First, the minimum size of a SLB is comparable with optical wavelengths. However, in most of the radiative processes considered previously, the finite-size effect of the bubble was neglected. In other words, the theory of radiative processes in extended space was used to discuss optical emission in a micrometer-sized SLB. It is not obvious

that this effect is negligible. Second, regions of extremely high densities and high temperatures are formed inside a SLB during its collapsing phase. Thus the bubble is highly inhomogeneous, and light waves generated from its interior would be scattered. Third, as mentioned above, a plasma shell could possibly develop inside a SLB [15], and the emission and propagation of electromagnetic waves could be strongly influenced by this plasma shell. In particular, the degree of ionization of the plasma and its plasma frequency are crucial factors determining the properties of the system.

In this paper we investigate the influences of the above-mentioned factors on the process of spontaneous emission. It is unlikely that spontaneous emission alone can explain all physical observations in SL, yet it serves as a simple model to illustrate the interplay between the radiative processes and the unusual environment existing in a SLB. It is well known that when an atomic system is placed in a small cavity, the decay rate of the system will be modified (enhanced or inhibited) owing to the changes in the density of states of photons, which is a measure of the spontaneous decay rate according to the Fermi golden rule [31–33]. Physically speaking, whereas the fields are uniform in an extended free space, the presence of the cavity redistributes the strengths of the fields, so that they are stronger at some points and weaker at others. Therefore, atoms at different locations may experience enhancement or inhibition in their spontaneous emission rates. For example, enhanced transition rates have been observed and reported for atoms in micrometer-sized dielectric spheres [34], which are of about the same size as the SL bubbles.

As a direct consequence of the rapid compression in a SLB, the gas density and the refractive index inside the bubble are strongly inhomogeneous. Hence it is likely that the electromagnetic fields would be distorted, leading to nontrivial effects on the process of spontaneous emission. In this paper, we will present a detailed study of the density of states of photons in spheres with multiple layers of different refractive indices, mimicking various stages of a SLB. In particular, we show that the decay rate could be strongly enhanced in the presence of a thin weakly ionized plasma shell inside the bubble, the existence of which was predicted recently in numerical simulations of a SLB as a result of shock formation [15]. The time scale of shock-wave formation is of tens of picoseconds, which is comparable to the duration of light pulses observed in SL. Thus our discovery suggests that the morphology of the plasma shell, as well as its composition, might be an important ingredient of the light-emitting mechanism in SL.

The organization of this paper is as follows. In Secs. II and III, we present the theory of normal mode expansion and quantization of the electromagnetic (EM) fields in a dielectric sphere embedded in another dielectric medium. In Sec. IV we then discuss the interactions between the EM fields and an atom inside the sphere. We calculate the decay rates of this system with the golden rule approximation, and show that they are proportional to the density of photon states. Generalization to multilayered spheres is carried out in Sec. V. We present a systematic and detailed study of the EM fields in a multilayered spherical cavity, and discuss the dependence of these fields on various parameters characterizing the system. The tools we developed in previous sections are then used in Sec. VI to calculate the EM fields in a multilayered SL bubble. Results from numerical hydrodynamic simulations [12,13] suggest that two scenarios, the emergence of compressional waves and shock waves, are of particular interest. In Sec. VII, we present results showing that the existence of a thin plasma shell, as induced perhaps by a shock wave [15], gives rise to a large enhancement in the EM fields and hence the spontaneous transition rates, which might play a crucial role in the phenomenon of SL. We summarize our main results and their implications in Sec. VIII.

II. NORMAL MODES OF EM FIELDS IN SPHERICAL GEOMETRY

Consider the EM field inside a dielectric sphere characterized by the dielectric constant $\epsilon(\mathbf{r})=n^2(\mathbf{r})$. Hereafter we shall assume that $\epsilon(\mathbf{r})$ is spherically symmetric, and hence it depends on the radius r only. The fields satisfy the Maxwell equations [35]

$$\nabla\cdot[\epsilon(\mathbf{r})\mathbf{E}]=0, \tag{2.1}$$

$$\nabla\cdot\mathbf{B}=0, \tag{2.2}$$

$$\nabla\times\mathbf{E}=-\frac{1}{c}\frac{\partial\mathbf{B}}{\partial t}, \tag{2.3}$$

$$\nabla\times\mathbf{B}=\frac{\epsilon(\mathbf{r})}{c}\frac{\partial\mathbf{E}}{\partial t}, \tag{2.4}$$

where c is the speed of light in vacuum, and we also assume that the magnetic susceptibility $\mu(\mathbf{r})$ is equal to 1, as it is for most nonmagnetic materials.

Let the vector and scalar potentials be $\mathbf{A}(\mathbf{r},t)$, and $\phi(\mathbf{r},t)$, respectively. In the absence of free charges and under the generalized Coulomb gauge condition,

$$\nabla\cdot[\epsilon(\mathbf{r})\mathbf{A}(\mathbf{r},t)]=0. \tag{2.5}$$

Then it can be shown that $\mathbf{A}(\mathbf{r},t)$ satisfies the vector wave equation

$$\nabla\times(\nabla\times\mathbf{A})+\frac{\epsilon(\mathbf{r})}{c^2}\frac{\partial^2\mathbf{A}}{\partial t^2}=0, \tag{2.6}$$

and $\phi(\mathbf{r},t)=0$. Hence the electric and magnetic fields are given by

$$\mathbf{E}(\mathbf{r},t)=-\frac{1}{c}\frac{\partial\mathbf{A}(\mathbf{r},t)}{\partial t} \tag{2.7}$$

and

$$\mathbf{B}(\mathbf{r},t)=\nabla\times\mathbf{A}(\mathbf{r},t), \tag{2.8}$$

respectively.

To look for normal mode solutions to Eq. (2.5), we further assume that

$$\mathbf{A}(\mathbf{r},t)=Q(t)\tilde{\mathbf{A}}(\mathbf{r}), \tag{2.9}$$

and we thus obtain the equations

$$\nabla\times[\nabla\times\tilde{\mathbf{A}}(\mathbf{r})]-\epsilon(\mathbf{r})k^2\tilde{\mathbf{A}}(\mathbf{r})=0, \tag{2.10}$$

$$\frac{d^2Q(t)}{dt^2}+\omega^2Q(t)=0, \tag{2.11}$$

where $k=\omega/c$.

The vector potential $\mathbf{A}(\mathbf{r},t)$ can then be expanded in terms of the transverse-electric (TE) and transverse-magnetic (TM) spherical vector wave components,

$$\mathbf{A}(\mathbf{r},t)=\sum_{klm}\left[q_{klm}^{(E)}(t)\mathbf{u}_{klm}^{(E)}(\mathbf{r})+q_{klm}^{(M)}(t)\mathbf{u}_{klm}^{(M)}(\mathbf{r})\right], \tag{2.12}$$

where $\mathbf{u}_{klm}^{(E)}(\mathbf{r})$ and $\mathbf{u}_{klm}^{(M)}(\mathbf{r})$ are the TE and TM solutions to Eq. (2.10), respectively, given by

$$\mathbf{u}_{klm}^{(E)}(\mathbf{r})=f_l^{(E)}(kr)\mathbf{X}_{lm}(\theta,\phi), \tag{2.13}$$

$$\mathbf{u}_{klm}^{(M)}(\mathbf{r})=\frac{i}{\epsilon(\mathbf{r})k}\nabla\times[f_l^{(M)}(kr)\mathbf{X}_{lm}(\theta,\phi)] \tag{2.14}$$

for $m\geqslant 0$, and

$$\mathbf{u}_{kl-m}^{(\lambda)}(\mathbf{r})=\mathbf{u}_{klm}^{*(\lambda)}(\mathbf{r}), \tag{2.15}$$

where $\lambda=E(M)$ for the TE (TM) case, and

$$\mathbf{X}_{lm}(\theta,\phi)\equiv\frac{(-i\mathbf{r}\times\nabla)Y_{lm}(\theta,\phi)}{\sqrt{l(l+1)}} \tag{2.16}$$

are the vector spherical harmonics. From Eq. (2.10), it is readily shown that the scalar function $\varphi_l^{(\lambda)}(r)=rf_l^{(\lambda)}(kr)$ satisfies the equation

$$\frac{d}{dr}\left[\rho(r)\frac{d\varphi_l^{(\lambda)}(r)}{dr}\right]+\rho(r)\left[\epsilon(r)k^2-\frac{l(l+1)}{r^2}\right]\varphi_l^{(\lambda)}(r)=0, \tag{2.17}$$

where $\rho(r)=1(\epsilon(r)^{-1})$ for the TE (TM) case.

Consider a dielectric sphere of radius a_1 and dielectric constant $\epsilon_1=n_1^2$, embedded in an ambient medium with dielectric constant $\epsilon_2=n_2^2$ as an example. It is readily shown from Eq. (2.17) that

$$f_l^{(E)}(kr)=\alpha_1^{(E)}h_l^{(1)}(n_1kr)+\beta_1^{(E)}h_l^{(2)}(n_1kr),\quad r<a_1, \tag{2.18}$$

$$f_l^{(E)}(kr)=\alpha_2^{(E)}h_l^{(1)}(n_2kr)+\beta_2^{(E)}h_l^{(2)}(n_2kr),\quad r>a_1, \tag{2.19}$$

$$f_l^{(M)}(kr)=\alpha_1^{(M)}h_l^{(1)}(n_1kr)+\beta_1^{(M)}h_l^{(2)}(n_1kr),\quad r<a_1, \tag{2.20}$$

$$f_l^{(M)}(kr)=\alpha_2^{(M)}h_l^{(1)}(n_2kr)+\beta_2^{(M)}h_l^{(2)}(n_2kr),\quad r>a_1, \tag{2.21}$$

where $\alpha_j^{(\lambda)}$ and $\beta_j^{(\lambda)}(j=1,2)$ are constants to be determined from the boundary conditions.

Matching appropriate boundary conditions at $r=a_1$, we find that

$$\alpha_2^{(E)}=\frac{in_2x_1^2}{2}\{W_{21}^{(E)}[h_l^{(1)}(n_1x_1),h_l^{(2)}(n_2x_1)]\alpha_1^{(E)}+W_{21}^{(E)}[h_l^{(2)}(n_1x_1),h_l^{(2)}(n_2x_1)]\beta_1^{(E)}\}, \tag{2.22}$$

$$\beta_2^{(E)}=-\frac{in_2x_1^2}{2}\{W_{21}^{(E)}[h_l^{(1)}(n_1x_1),h_l^{(1)}(n_2x_1)]\alpha_1^{(E)}+W_{21}^{(E)}[h_l^{(2)}(n_1x_1),h_l^{(1)}(n_2x_1)]\beta_1^{(E)}\}, \tag{2.23}$$

$$\alpha_2^{(M)}=\frac{in_2^3x_1^2}{2}\{W_{21}^{(M)}[h_l^{(1)}(n_1x_1),h_l^{(2)}(n_2x_1)]\alpha_1^{(M)}+W_{21}^{(M)}[h_l^{(2)}(n_1x_1),h_l^{(2)}(n_2x_1)]\beta_1^{(M)}\}, \tag{2.24}$$

$$\beta_2^{(M)}=-\frac{in_2^3x_1^2}{2}\{W_{21}^{(M)}[h_l^{(1)}(n_1x_1),h_l^{(1)}(n_2x_1)]\alpha_1^{(M)}+W_{21}^{(M)}[h_l^{(2)}(n_1x_1),h_l^{(1)}(n_2x_1)]\beta_1^{(M)}\}, \tag{2.25}$$

where $x_1=ka_1$. In the above equations, we define the Wronskians as

$$W_{21}^{(E)}(f,g)=fg'-f'g, \tag{2.26}$$

$$W_{21}^{(M)}(f,g)=\frac{fg'}{n_2^2}-\frac{f'g}{n_1^2}+\left(\frac{1}{n_2^2}-\frac{1}{n_1^2}\right)\frac{fg}{x_1}, \tag{2.27}$$

with $'\equiv d/dx_1$.

The regularity of the solution at the origin leads to the following relation:

$$\alpha_1^{(\lambda)}=\beta_1^{(\lambda)}=\frac{1}{2}\gamma^{(\lambda)}. \tag{2.28}$$

It is also easy to verify that

$$|\alpha_2^{(\lambda)}|=|\beta_2^{(\lambda)}|, \tag{2.29}$$

which is consistent with the law of energy conservation.

In order to define the normal modes of this system, which are essential for the formulation of a quantized field theory, a perfectly conducting spherical shell is placed at a large distance $r=R$. Eventually, we shall take the limit $R\to\infty$. The allowed values of k (ω) are hence discretized by the imposed boundary conditions, which require that both the transverse component of the electric field and the longitudinal component of the magnetic field vanish on the surface of the metal sphere, i.e.,

$$\mathbf{E}_{\parallel}(R)=0, \tag{2.30}$$

$$\mathbf{B}_{\perp}(R)=0. \tag{2.31}$$

This is equivalent to imposing the conditions

$$f_l^{(E)}(R)=0, \tag{2.32}$$

$$\frac{d}{dr}(rf_l^{(M)})|_R=0. \tag{2.33}$$

Upon imposing these boundary conditions at $r=R$, the eigenfrequencies of the EM field normal modes can be found. For example, in the TE case,

$$\omega_{\nu lE} \equiv k_{\nu lE} c = \left(\nu + \frac{1}{2} \right) \frac{\pi c}{n_2 R} - \frac{c}{n_2 R} \delta_E(l,\nu), \quad (2.34)$$

where $\nu = 0,1,2,\ldots$ is the radial quantum number, and $\delta_E(l,\nu)$ is a phase angle of order unity. Therefore, the frequencies are spaced by

$$\triangle \omega = \frac{\pi c}{n_2 R} + O(R^{-2}). \quad (2.35)$$

With this expansion, the general solution of the vector potential can be written as

$$\mathbf{A}(\mathbf{r},t) = \sum_{\nu lm} q^{(E)}_{\nu lm}(t) f^{(E)}_l(k_{\nu lE} r) \mathbf{X}_{lm}(\theta,\phi) + \sum_{\nu lm} \frac{i}{\epsilon k_{\nu lM}} q^{(M)}_{\nu lm}(t) \boldsymbol{\nabla} \times [f^{(M)}_l(k_{\nu lM} r) \mathbf{X}_{lm}(\theta,\phi)]. \quad (2.36)$$

The electric and magnetic fields can be expanded similarly as

$$\mathbf{E}(\mathbf{r},t) = -\frac{1}{c} \sum_{\nu lm} \left\{ \dot{q}^{(E)}_{\nu lm}(t) f^{(E)}_l(k_{\nu lE} r) \mathbf{X}_{lm}(\theta,\phi) + \frac{i}{\epsilon k_{\nu lM}} \dot{q}^{(M)}_{\nu lm}(t) \boldsymbol{\nabla} \times [f^{(M)}_l(k_{\nu lM} r) \mathbf{X}_{lm}(\theta,\phi)] \right\} \quad (2.37)$$

and

$$\mathbf{B}(\mathbf{r},t) = \sum_{\nu lm} \{ q^{(E)}_{\nu lm}(t) \boldsymbol{\nabla} \times [f^{(E)}_l(k_{\nu lE} r) \mathbf{X}_{lm}(\theta,\phi)] + i k_{\nu lM} q^{(M)}_{\nu lm}(t) f^{(M)}_l(k_{\nu lM} r) \mathbf{X}_{lm}(\theta,\phi) \}. \quad (2.38)$$

Furthermore, $\alpha^{(E)}_2$ and $\alpha^{(M)}_2$ can be deduced from the orthonormal relation

$$\frac{1}{4\pi c^2} \int_R \epsilon(\mathbf{r}) \mathbf{u}^{(\lambda)}_{\nu lm}(\mathbf{r}) \mathbf{u}^{*(\lambda')}_{\nu' l' m'}(\mathbf{r}) d\mathbf{r} = \delta_{\nu\nu'} \delta_{ll'} \delta_{mm'} \delta_{\lambda\lambda'}, \quad (2.39)$$

and the asymptotic forms of the Hankel functions, yielding the results

$$|\alpha^{(E)}_2|^2 = |\beta^{(E)}_2|^2 = \frac{2\pi n_2 c^2 k^2}{R}, \quad (2.40)$$

$$|\alpha^{(M)}_2|^2 = |\beta^{(M)}_2|^2 = \frac{2\pi n_2^3 c^2 k^2}{R}. \quad (2.41)$$

III. QUANTIZATION OF EM FIELDS IN SPHERICAL GEOMETRY

The quantization of the EM fields in a spherically symmetric system begins with the normal mode expansion of $\mathbf{A}(\mathbf{r},t)$ [36],

$$\mathbf{A}(\mathbf{r},t) = \sum_{\nu lm\lambda} q_{\nu lm\lambda}(t) \mathbf{u}^{(\lambda)}_{\nu lm}(\mathbf{r}), \quad (3.1)$$

where $\mathbf{u}(\mathbf{r})$ are the mode functions of a general system and the q's are the generalized coordinates of the fields, which satisfy Eq. (2.11). Note that

$$q_{\nu l,m\lambda}(t) = q^*_{\nu l,-m\lambda}(t), \quad (3.2)$$

following directly from the reality of $\mathbf{A}(\mathbf{r},t)$.

The Lagrangian of the system, defined by

$$L = \frac{1}{8\pi} \int_0^R [\epsilon(\mathbf{r}) \mathbf{E}^2 - \mathbf{B}^2] d\mathbf{r}, \quad (3.3)$$

assumes the form

$$L = \frac{1}{2} \sum_{\nu lm\lambda} [\dot{q}_{\nu lm\lambda}(t) \dot{q}^*_{\nu lm\lambda}(t) - \omega^2_{\nu l\lambda} q_{\nu lm\lambda}(t) q^*_{\nu lm\lambda}(t)] \quad (3.4)$$

by the orthogonality of $\mathbf{u}^{(\lambda)}_{\nu lm}(\mathbf{r})$. Therefore, the conjugate momentum of $q_{\nu lm\lambda}$ is given by

$$p_{\nu lm\lambda}(t) = \frac{\partial L}{\partial \dot{q}_{\nu lm\lambda}} = \dot{q}^*_{\nu lm\lambda}(t). \quad (3.5)$$

As in Eq. (3.2), the conjugate momenta obey the relation

$$p_{\nu lm\lambda}(t) = p^*_{\nu l,-m\lambda}(t). \quad (3.6)$$

In terms of these generalized coordinates and momenta, the Hamiltonian of the system can be expressed as

$$H = \sum_{\nu lm\lambda} p_{\nu lm\lambda} \dot{q}_{\nu lm\lambda} - L, \quad (3.7)$$

$$= \frac{1}{2} \sum_{\nu lm\lambda} [p_{\nu lm\lambda} p^*_{\nu lm\lambda} + \omega^2_{\nu l\lambda} q_{\nu lm\lambda} q^*_{\nu lm\lambda}]. \quad (3.8)$$

The generalized coordinates $q_{\nu lm\lambda}$ can be expressed as a sum of two independent solutions

$$q_{\nu lm\lambda}(t) = \sqrt{\frac{\hbar}{2\omega_{\nu l\lambda}}} [a^*_{\nu l,-m\lambda}(t) + a_{\nu lm\lambda}(t)], \quad (3.9)$$

following directly from the equation of motion (2.11), with

$$a_{\nu lm\lambda}(t) = a_{\nu lm\lambda}(0) e^{-i\omega_{\nu l\lambda} t} \quad (3.10)$$

and

$$a^*_{\nu lm\lambda}(t) = a^*_{\nu lm\lambda}(0) e^{i\omega_{\nu l\lambda} t}. \quad (3.11)$$

Similarly, the conjugate momenta are given by

$$p_{\nu lm\lambda}(t)=i\sqrt{\frac{\hbar\omega_{\nu l\lambda}}{2}}[a^*_{\nu lm\lambda}(t)-a_{\nu l,-m\lambda}(t)]. \quad (3.12)$$

To quantize the EM field of the system, we impose the following commutation relations on the generalized coordinates and their conjugate momenta [36]:

$$[\hat{q}_{\nu lm\lambda},\hat{q}_{\nu' l' m'\lambda'}]=[\hat{p}_{\nu lm\lambda},\hat{p}_{\nu' l' m'\lambda'}]=0, \quad (3.13)$$

$$[\hat{q}_{\nu lm\lambda},\hat{p}_{\nu' l' m'\lambda'}]=i\hbar\,\delta_{\nu\nu'}\delta_{ll'}\delta_{mm'}\delta_{\lambda\lambda'}. \quad (3.14)$$

From the definitions of the a's and $a^\dagger$'s, their commutation relations follow immediately:

$$[\hat{a}_{\nu lm\lambda}(t),\hat{a}^\dagger_{\nu' l' m'\lambda'}(t)]=\delta_{\nu\nu'}\delta_{ll'}\delta_{mm'}\delta_{\lambda\lambda'}, \quad (3.15)$$

$$[\hat{a}_{\nu lm\lambda}(t),\hat{a}_{\nu' l' m'\lambda'}(t)]=[\hat{a}^\dagger_{\nu lm\lambda}(t),\hat{a}^\dagger_{\nu' l' m'\lambda'}]=0. \quad (3.16)$$

Note that the c numbers q's, p's, a's, and a^*'s are now promoted to operators $\hat{q}$'s, $\hat{p}$'s, $\hat{a}$'s and $\hat{a}^\dagger$'s respectively. As usual, $\hat{a}_s$ and $\hat{a}^\dagger_s$ ($s=\{\nu lm\lambda\}$) are the annihilation and creation operators of photons in the s mode, respectively. In terms of these operators, the vector potential becomes a field operator and can be written as

$$\hat{\mathbf{A}}(\mathbf{r},t)=\sum_{\nu lm\lambda}\frac{1}{\sqrt{2\hbar\omega_{\nu l\lambda}}}[\hat{a}_{\nu lm\lambda}(t)\mathbf{u}^{(\lambda)}_{\nu lm}(\mathbf{r}) + \hat{a}^\dagger_{\nu lm\lambda}(t)\mathbf{u}^{(\lambda)*}_{\nu lm}(\mathbf{r})]. \quad (3.17)$$

IV. FIELD-ATOM INTERACTION

For the purpose of illustration and simplicity, we first consider a two-level atom situated at $\mathbf{r}_0$ in a dielectric sphere of radius a_1 and dielectric constant $\epsilon_1=n_1^2$ surrounded by another uniform medium of dielectric constant $\epsilon_2=n_2^2$. The Hamiltonian of the system is [36]

$$\hat{H}=\frac{1}{2}\hbar\omega_0\hat{\sigma}_z+\sum_s\hbar\omega_s\hat{a}^\dagger_s\hat{a}_s+\hat{H}_{\rm int}, \quad (4.1)$$

where $\hat{\sigma}_z$ is the Pauli matrix, $\omega_0\equiv k_0c$ is the frequency difference between the two atomic levels, and

$$\hat{H}_{\rm int}\equiv-\hat{\mathbf{p}}\cdot\hat{\mathbf{E}}(\mathbf{r}_0), \quad (4.2)$$

with $\hat{\mathbf{p}}$ being the electric dipole operator of the atom.

The transition rate w can be calculated using Fermi's golden rule, which is valid if the interactions are sufficiently weak,

$$w=\frac{2\pi}{\hbar^2}\sum_s|\langle gs|\hat{H}_{\rm int}|u0\rangle|^2\delta(\omega_s-\omega_0), \quad (4.3)$$

where $|gs\rangle$ represents the state in which the atom is in the lower energy level, and one photon is in mode s, while $|u0\rangle$ represents the state with the atom excited to its upper level and no photon. The δ function in Eq. (4.3) is the result of Fermi's golden rule, which states that all significant transitions conserve energy.

We define two matrices P_{ij} and E_{ij} by

$$P_{ij}=\langle g|\hat{p}_i|u\rangle\langle g|\hat{p}_j|u\rangle^*, \quad (4.4)$$

$$E_{ij}=\frac{1}{4\pi\hbar\omega_0}\sum_s e^*_{i,s}e_{j,s}\delta(\omega_s-\omega_0), \quad (4.5)$$

where $e_{i,s}$ represents the ith component of $\langle s|\hat{\mathbf{E}}|0\rangle$, and the subscripts i and j can be r,θ, or ϕ. Hence

$$w=\frac{8\pi^2\omega_0}{\hbar}\sum_{i,j}P_{ij}E_{ij}. \quad (4.6)$$

While P_{ij} depends on the details (strengths and orientations) of the emitting atom, E_{ij} is a measure of the fluctuations of the vacuum electric field, which can be strongly affected by the dielectric medium. The main objective of the present paper is to study how E_{ij}, and hence the transition rate w, can be modified due to the unusual environment (high pressure and high temperature) encountered in a SLB.

Explicit expressions of E_{ij} can be obtained from simple algebra using the facts that $\Sigma_s=\Sigma_\nu\Sigma_{l,m}\Sigma_\lambda$ and in the $R\to\infty$ limit, $\Sigma_\nu\to(R/\pi c)\int d\omega_s$. Using the results obtained in Secs. II and III, we can show that (i) for $r<a_1$,

$$E_{rr}=\frac{R}{16\pi^3c\hbar\omega_0}\sum_l l^2(l+1)^2(2l+1)\frac{|\gamma^{(M)}|^2j_l(n_1k_0r_0)^2}{n_1^4k_0^2r_0^2}, \quad (4.7)$$

$$E_{\theta\theta}=\frac{R}{32\pi^3c\hbar\omega_0}\sum_l l(l+1)(2l+1)\left\{|\gamma^{(E)}|^2j_l(n_1k_0r_0)^2 + \frac{|\gamma^{(M)}|^2}{n_1^4k_0^2r_0^2}\left[r_0\frac{dj_l(n_1k_0r)}{dr}\bigg|_{r=r_0}+j_l(n_1k_0r_0)\right]^2\right\}, \quad (4.8)$$

$$E_{\phi\phi}=E_{\theta\theta}; \quad (4.9)$$

and (ii) for $r>a_1$,

$$E_{rr}=\frac{R}{16\pi^3c\hbar\omega_0}\sum_l l^2(l+1)^2(2l+1) \times\frac{|\alpha_2^{(M)}h_l^{(1)}(n_2k_0r_0)+\beta_2^{(M)}h_l^{(2)}(n_2k_0r_0)|^2}{n_2^4k_0^2r_0^2}, \quad (4.10)$$

$$E_{\theta\theta}=\frac{R}{32\pi^3 c\hbar\omega_0}\sum_l l(l+1)(2l+1)$$
$$\times\Bigg\{|\alpha_2^{(E)}h_l^{(1)}(n_2k_0r_0)+\beta_2^{(E)}h_l^{(2)}(n_2k_0r_0)|^2$$
$$+\frac{1}{n_2^4k_0^2r_0^2}\Bigg|r_0\frac{d}{dr}[\alpha_2^{(M)}h_l^{(1)}(n_2k_0r)$$
$$+\beta_2^{(M)}h_l^{(2)}(n_2k_0r)]_{r=r_0}+\alpha_2^{(M)}h_l^{(1)}(n_2k_0r_0)$$
$$+\beta_2^{(M)}h_l^{(2)}(n_2k_0r_0)\Bigg|^2\Bigg\}, \tag{4.11}$$

$$E_{\phi\phi}=E_{\theta\theta}; \tag{4.12}$$

and (iii) $E_{ij}=0$ for $i\neq j$. Note that in the above equations E_{ij} consists of two independent contributions from the TE and TM modes.

The spontaneous emission rate of a dipole is most generally given by Eq. (4.6). For example, if the dipole is in the radial direction, then

$$w=\frac{4\pi^2\omega_0}{\hbar}P_{rr}E_{rr}. \tag{4.13}$$

It is convenient for us to normalize the emission rate by that in the extended vacuum, which is given by

$$w_{\rm vac}=\frac{4p^2\omega_0^3}{3\hbar c^3}, \tag{4.14}$$

where $p=(\Sigma_i P_{ii})^{1/2}$ is the electric dipole strength. Hence, using Eq. (4.6), the normalized emission rate $w_n\equiv w/w_{\rm vac}$ is

$$w_n=\frac{6\pi^2c^3}{\omega_0^2}E_{rr}. \tag{4.15}$$

Similar expressions can be obtained for dipoles tangential to the surface of the sphere, namely,

$$w_n=\frac{6\pi^2c^3}{\omega_0^2}E_{tt}, \tag{4.16}$$

where $E_{tt}\equiv(E_{\theta\theta}+E_{\phi\phi})/2=E_{\theta\theta}=E_{\phi\phi}$.

Figure 1 shows the transition rates as a function of ω_0 for a randomly oriented radiating dipole situated at $r_0/r_1=0.1$ and 0.9 of a uniform bubble ($n_1=1$) surrounded by water ($n_2=1.33$). We note that the transition rates, given by

$$w_n=\frac{2\pi^2c^3}{\omega_0^2}(E_{rr}+E_{\theta\theta}+E_{\phi\phi}), \tag{4.17}$$

are nonuniform and fluctuate slightly around unity. A small enhancement can be observed for some particular frequencies, while, for others, the transition rate is inhibited. Nevertheless, we expect that for such an air bubble in water, where

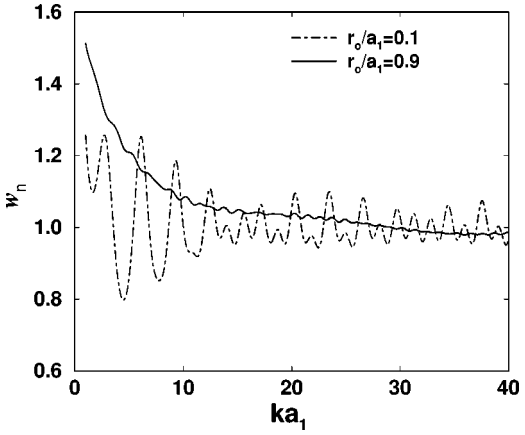

FIG. 1. Normalized emission rate of a dipole inside a gas bubble embedded in water, vs the transition frequency. The solid line shows the enhancement experienced by a dipole placed near the boundary of the bubble, at $r_0=0.9a_1$, where r_0 and a_0 are the distance of the dipole from the center and the radius of the bubble, respectively. The dotted line shows that of a dipole placed near the center, at $r_0=0.1a_0$. No significant enhancement is observed in both cases.

n_1 is less than n_2, the enhancement is never prominent for all frequencies, regardless of the location and the direction of the dipole.

However, the results are somewhat different when we consider the opposite case, where n_1 is greater than n_2, e.g., a water droplet in vacuum or air. It is well known that light waves propagating in a dense medium will be totally reflected at the interface between two media. Hence light waves will be trapped inside the sphere of higher refractive index (n_1 in the present situation) and form metastable states, called morpholgy-dependent resonances (MDR's) [37], at appropriate frequencies. These MDR's can strongly alter the vacuum fluctuations of EM fields, and hence introduce nontrivial effects on a radiating atom inside the sphere [32–34]. In order to have a glimpse of the effects of these MDR's on the transition rates, in what follows we study a simple case with $n_1=1.33$ and $n_2=1.00$. In Fig. 2, the ra-

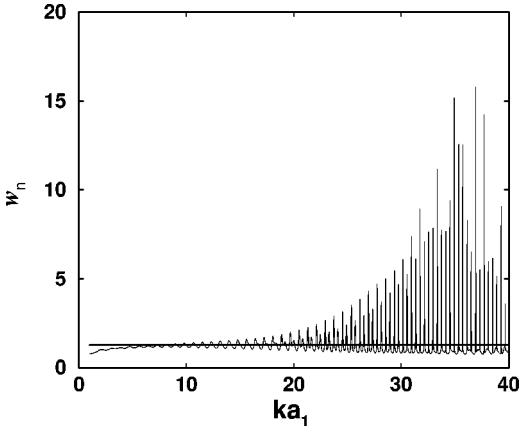

FIG. 2. Normalized emission rate for a dipole near the surface of a water droplet in air ($r_0/a_1=0.9$). Sharp enhancement due to MDR's are observed, but a spectral averaging reduces the enhancement to the order of 1. The horizontal line shows the spectral average.

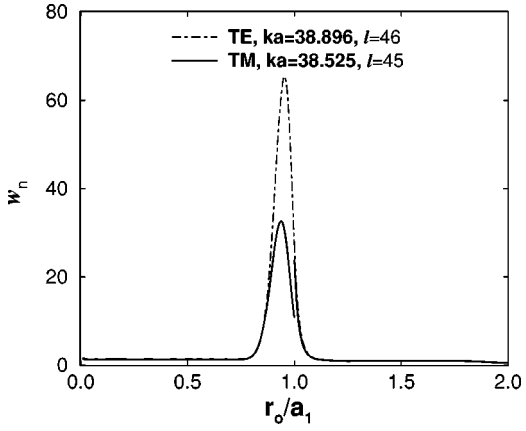

FIG. 3. Spatial dependence of the normalized emission rate for a TE mode ($ka_1=38.896, l=46$) and a TM mode ($ka_1=38.525, l=45$), at resonance frequency. The enhancement is peaked at the boundary of the sphere, due to the localization of photons trapped by total internal reflection. The enhancement of the TE mode is continuous across the boundary, while that of the TM mode is not. This is due to the discontinuity in the normal component of the electric field of TM modes across the boundary.

diation rate for a dipole near the surface ($r_0/a_1=0.9$) is plotted against ka. We find that the transition rate is mildly enhanced for some particular frequencies and inhibited for others, which is similar to the results for an air bubble. However, there are also many sharp spikes in Fig. 2, indicating strong enhancement at certain frequencies. Physically speaking, these frequencies correspond to eigenfrequencies of MDR's, whose lifetimes are inversely proportional to the widths of the respective spikes. As shown in Fig. 3, the enhancement is particularly pronounced for dipoles close to the interface, and is suppressed for dipoles located near the center. This can be understood as follows. Total internal reflection can take place only when the incident angle exceeds the critical angle, and hence photons (or light waves) reflected from the interface are confined to a region close to the interface. As a result, the fields there will be stronger than that near the center. We also note that the transition rate as a function of radius at the resonance frequencies of MDR's is discontinuous across the interface for the TM modes, reflecting the discontinuity in the normal component of **E** there; for the TE MDR's, conversely, the transition rate remains continuous.

For such a system to have marked enhancement in the visible range of the emission spectrum at the MDR frequencies, its radius should be of the order of several micrometers, because our results show that the resonance effect is too weak for $ka<10$. As mentioned previously, the size of a SLB is also of the order of several micrometers, we therefore expect that the formation of MDR's could be of relevance to the emission mechanism of a SLB. However, as total internal reflection is an essential means to confine light waves inside the system, it seems unlikely that MDR's, especially those with small leakage rates and hence a strong enhancing effect, could be formed in a uniform bubble ($n_1\approx 1$) surrounded by water ($n_2\approx 1.33$). It is only the extreme physical conditions generated in the collapsing phase of a SLB that give rise to MDR's yielding strong enhancement. We shall discuss this issue in Sec. V.

V. GENERALIZATION TO LAYERED SPHERES

Many theoretical and numerical studies on SL strongly suggest that in the drastic collapsing phase of a SLB, the density of air in a thin layer of the bubble could be as high as 1000 times that under standard conditions [10–14,38], i.e., almost the same as the density of water. Some of these studies even confirm the emergence of shock waves [10–14,38] with very thin but dense shock fronts. More importantly, the gas molecules (atoms) become potential light emitters under such high temperature. Moreover, under these conditions, a fraction of the molecules (atoms) inside may be ionized and a thin plasma shell could be formed [11,14,15]. The difference in density and the formation of a thin plasma shell could both contribute to the spatial variance of the dielectric constant of the bubble. In order to study the emission mechanism in a SLB with a spatially varying dielectric constant, we consider, for simplicity, the spontaneous decay rates of molecules (atoms) in a multilayered sphere. We also note that despite its high velocity, this shell can be considered static when compared with an optical time scale, and hence our model is applicable.

The mathematics used to handle a multilayered sphere is similar to that presented in Sec. IV, and a transfer matrix formalism will be developed to handle the reflections and transmissions of waves at the interfaces $r=a_1, a_2, \ldots (a_1<a_2<\cdots)$.

In the jth layer ($j=1,2,\ldots$) the mode functions for the two polarizations are given by

$$f_l^{(E)}(r)=\alpha_j^{(E)}h_l^{(1)}(n_jkr)+\beta_j^{(E)}h_l^{(2)}(n_jkr), \tag{5.1}$$

$$f_l^{(M)}(r)=\alpha_j^{(M)}h_l^{(1)}(n_jkr)+\beta_j^{(M)}h_l^{(2)}(n_jkr), \tag{5.2}$$

where n_j is the refractive index of the layer. For an interface separating two layers say, layer 1 and layer 2 at $r=a_1$, we define the transfer matrices

$$T_{21}^{(E)}=\frac{in_2x_1^2}{2}\begin{pmatrix} W_{21}^{(E)}[h_l^{(1)}(n_1x_1),h_l^{(2)}(n_2x_1)] & W_{21}^{(E)}[h_l^{(2)}(n_1x_1),h_l^{(2)}(n_2x_1)] \\ -W_{21}^{(E)}[h_l^{(1)}(n_1x_1),h_l^{(1)}(n_2x_1)] & -W_{21}^{(E)}[h_l^{(2)}(n_1x_1),h_l^{(1)}(n_2x_1)] \end{pmatrix}, \tag{5.3}$$

$$T_{21}^{(M)}=\frac{in_2^3x_1^2}{2}\begin{pmatrix} W_{21}^{(M)}[h_l^{(1)}(n_1x_1),h_l^{(2)}(n_2x_1)] & W_{21}^{(M)}[h_l^{(2)}(n_1x_1),h_l^{(2)}(n_2x_1)] \\ -W_{21}^{(M)}[h_l^{(1)}(n_1x_1),h_l^{(1)}(n_2x_1)] & -W_{21}^{(M)}[h_l^{(2)}(n_1x_1),h_l^{(1)}(n_2x_1)] \end{pmatrix}, \tag{5.4}$$

where $W^{(E)}$ and $W^{(M)}$ are defined as in Eqs. (2.26) and (2.27). By matching the boundary conditions at $r=a_1$ as sketched in

Sec. II, and adopting the definitions of the transfer matrices, the incoming and outgoing wave amplitudes in the two layers can be concisely related as follows:

$$\begin{pmatrix} \alpha_2^{(\lambda)} \\ \beta_2^{(\lambda)} \end{pmatrix} = T_{21}^{(\lambda)} \begin{pmatrix} \alpha_1^{(\lambda)} \\ \beta_1^{(\lambda)} \end{pmatrix}. \tag{5.5}$$

To illustrate our method, we specifically consider a dielectric sphere with a central core and an outer layer with different dielectric constants. The central core has a refractive index n_1 and a radius a_1, and the outer layer, with thickness a_2-a_1, has a refractive index n_2. In other words, a_2 is the radius of the whole sphere, which is embedded in an infinite dielectric medium with a refractive index n_3.

Direct application of the tranfer matrix theory at the interface $r=a_2$ yields

$$\begin{pmatrix} \alpha_3^{(\lambda)} \\ \beta_3^{(\lambda)} \end{pmatrix} = T_{32}^{(\lambda)} \begin{pmatrix} \alpha_2^{(\lambda)} \\ \beta_2^{(\lambda)} \end{pmatrix}, \tag{5.6}$$

where

$$T_{32}^{(E)} = \frac{in_3x_2^2}{2} \begin{pmatrix} W_{32}^{(E)}[h_l^{(1)}(n_2x_2), h_l^{(2)}(n_3x_2)] & W_{32}^{(E)}[h_l^{(2)}(n_2x_2), h_l^{(2)}(n_3x_2)] \\ -W_{32}^{(E)}[h_l^{(1)}(n_2x_2), h_l^{(1)}(n_3x_2)] & -W_{32}^{(E)}[h_l^{(2)}(n_2x_2), h_l^{(1)}(n_3x_2)] \end{pmatrix}, \tag{5.7}$$

$$T_{32}^{(M)} = \frac{in_3^3x_2^2}{2} \begin{pmatrix} W_{32}^{(M)}[h_l^{(1)}(n_2x_2), h_l^{(2)}(n_3x_2)] & W_{32}^{(M)}[h_l^{(2)}(n_2x_2), h_l^{(2)}(n_3x_2)] \\ -W_{32}^{(M)}[h_l^{(1)}(n_2x_2), h_l^{(1)}(n_3x_2)] & -W_{32}^{(M)}[h_l^{(2)}(n_2x_2), h_l^{(1)}(n_3x_2)] \end{pmatrix}, \tag{5.8}$$

and $x_2=ka_2$.

Together with Eq. (5.5), we have

$$\begin{pmatrix} \alpha_3^{(\lambda)} \\ \beta_3^{(\lambda)} \end{pmatrix} = T_{32}^{(\lambda)} T_{21}^{(\lambda)} \begin{pmatrix} \alpha_1^{(\lambda)} \\ \beta_1^{(\lambda)} \end{pmatrix}. \tag{5.9}$$

Thus, by inverting the matrices, all unknown amplitudes can be expressed in terms of $\alpha_3^{(\lambda)}$ and $\beta_3^{(\lambda)}$, whose amplitudes can be determined from the normalization condition (2.39), requiring

$$|\alpha_3^{(E)}|^2 = |\beta_3^{(E)}|^2 = \frac{2\pi n_3 c^2 k^2}{R}, \tag{5.10}$$

$$|\alpha_3^{(M)}|^2 = |\beta_3^{(M)}|^2 = \frac{2\pi n_3^3 c^2 k^2}{R}. \tag{5.11}$$

The phase difference can be evaluated from the regularity condition at the origin, which requires $\alpha_1^{(\lambda)}=\beta_1^{(\lambda)}=\frac{1}{2}\gamma^{(\lambda)}$. Therefore, leaving alone an unimportant common phase factor, all coefficients can be solved from the above two matrix equations.

This transfer matrix method could be used to handle spheres consisting of arbitrary numbers of layers. Another example we will consider in this paper is a dielectric sphere with a central core with refractive index n_1 and radius a_1, and two outer layers with refractive indices n_2 and n_3 and thicknesses a_2-a_1 and a_3-a_2, respectively. The sphere is embedded in an extended dielectric medium with a refractive index n_4. Following similar steps as sketched above, we show that the wave amplitudes in each layer can be expressed in terms of those in the extended dielectric medium, i.e., $\alpha_4^{(\lambda)}$ and $\beta_4^{(\lambda)}$. For example, the following equation relates the wave amplitudes in the core to $\alpha_4^{(\lambda)}$ and $\beta_4^{(\lambda)}$:

$$\begin{pmatrix} \alpha_4^{(\lambda)} \\ \beta_4^{(\lambda)} \end{pmatrix} = T_{43}^{(\lambda)} T_{32}^{(\lambda)} T_{21}^{(\lambda)} \begin{pmatrix} \alpha_1^{(\lambda)} \\ \beta_1^{(\lambda)} \end{pmatrix}, \tag{5.12}$$

where

$$T_{43}^{(E)} = \frac{in_4x_3^2}{2} \begin{pmatrix} W_{43}^{(E)}[h_l^{(1)}(n_3x_3), h_l^{(2)}(n_4x_3)] & W_{43}^{(E)}[h_l^{(2)}(n_3x_3), h_l^{(2)}(n_4x_3)] \\ -W_{43}^{(E)}[h_l^{(1)}(n_3x_3), h_l^{(1)}(n_4x_3)] & -W_{43}^{(E)}[h_l^{(2)}(n_3x_3), h_l^{(1)}(n_4x_3)] \end{pmatrix}, \tag{5.13}$$

$$T_{43}^{(M)} = \frac{in_4^3x_3^2}{2} \begin{pmatrix} W_{43}^{(M)}[h_l^{(1)}(n_3x_3), h_l^{(2)}(n_4x_3)] & W_{43}^{(M)}[h_l^{(2)}(n_3x_3), h_l^{(2)}(n_4x_3)] \\ -W_{43}^{(M)}[h_l^{(1)}(n_3x_3), h_l^{(1)}(n_4x_3)] & -W_{43}^{(M)}[h_l^{(2)}(n_3x_3), h_l^{(1)}(n_4x_3)] \end{pmatrix}, \tag{5.14}$$

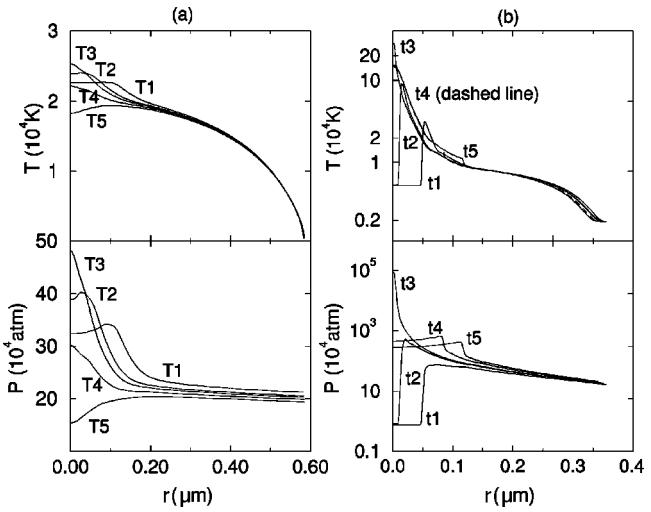

FIG. 4. Snapshots of the spatial profiles of pressure P and temperature T for an air bubble driven with a sound amplitude of $P_a = 1.35$ atm. (a) Results with the van der Waals gas equation of state (VEOS) are shown at $T_1 = 18$ ps, $T_2 = 20.1$ ps, $T_3 = 21$ ps, $T_4 = 22.1$ ps, and $T_5 = 24$ ps, taking the time at minimun bubble radius as zero. (b) Same as (a), but with nitrogen gas equation of state (NEOS) and $t_1 = -26.6$ ps, $t_2 = -23.9$ ps, $t_3 = -23.5$ ps, $t_4 = -20.4$ ps, and $t_5 = -18.4$ ps. The shock front moves inward toward $r = 0$ at t_1 and t_2, and outward at t_4 and t_5.

and $x_3 = ka_3$. Likewise, the normalization condition yields the results

$$|\alpha_4^{(E)}|^2 = |\beta_4^{(E)}|^2 = \frac{2\pi n_4 c^2 k^2}{R}, \tag{5.15}$$

$$|\alpha_4^{(M)}|^2 = |\beta_4^{(M)}|^2 = \frac{2\pi n_4^3 c^2 k^2}{R}, \tag{5.16}$$

and the EM fields are in turn completely determined. In what follows we apply our formulation developed so far to analyze the phenomenon of spontaneous decay in a SLB based on multilayered SLB models motivated by numerical hydrodynamic simulations.

VI. MULTILAYERED SLB MODELS

The extraordinary environments inside a SLB obviously rule out any models based on homogeneous dielectric spheres, let alone their inability to provide significant enhancements in the EM fields. Some numerical hydrodynamic models show the existence of compressional waves in various stages of the evolution of the SLB, and even shock waves, especially when the bubble approaches its minimum radius. In other words, it would be much more realistic to model a SLB as a multilayered dielectric sphere, instead of a uniform bubble as discussed in Sec. IV.

From the results of numerical simulations performed by Cheng and co-workers [12,13], shown in Fig. 4, the density of the argon gas could reach the order of 1 g cm^{-3} (i.e., about the same as the density of water) inside the dense region, while the gas outside could be much lower than this value. We will estimate the dielectric constant in the dense region by the Clausius-Mossotti equation and, for simplicity, assume the dielectric constant outside the dense region to be 1. The Clausius-Mossotti equation reads [35]

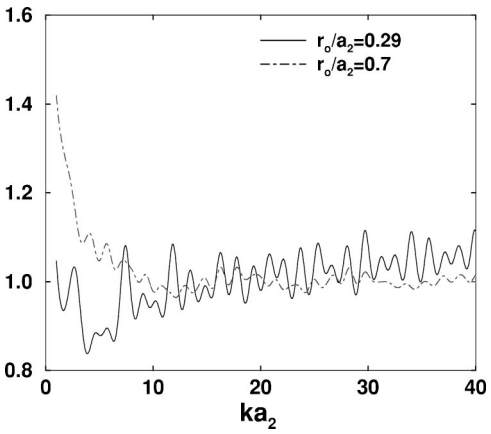

FIG. 5. Normalized emission rate of a dipole inside a gas bubble with compressional waves, which has a dense core with $n_1 = 1.16$ and radius $a_1 = 0.3a_2$ (a_2 is the radius of the whole bubble); and an outer layer with $n_2 = 1$. The ambient medium is water. The solid and dashed lines represent the normalized emission rate in the core at $r_0 = 0.29a_2$ and in the outer layer at $r_0 = 0.7a_2$, respectively. In both cases, no significant enhancement is observed.

$$\eta_{\mathrm{mol}} = \frac{3}{4\pi N}\left(\frac{\epsilon - 1}{\epsilon + 2}\right), \tag{6.1}$$

where η_{mol} is the molecular polarizability, and N the number of molecules per unit volume. Consider a SLB of argon gas. For argon at 0 °C and 1 atm, the refractive index at the sodium D line wavelength (5893 Å) is $1 + 2.837 \times 10^{-4}$. Assuming that the mass density of the dense region of argon to be 1 g cm^{-3}, we find that the refractive index there is about 1.16.

From Fig. 4, we observe that at some stages of SL, compressional waves may develop inside the bubble. Here we consider a simplified model in which a SLB consists of a central core with $a_1/a_2 = 0.3$ and a refractive index $n_1 = 1.16$, and an outer layer with thickness $0.7a_2$ and a refractive index 1. The normalized emission rate is plotted as a function of frequency in Fig. 5, from which we conclude that for such a bubble, the enhancement is only of order unity regardless of the location of the dipole. Note the absence of the sharp peaks corresponding to total internal reflection, which suggests that this effect is negligible because the ratio of the refractive indices across the boundary, being 1.16, is not large enough to produce significant MDR's. In this model, the gas inside the outer layer is assumed to be under ordinary pressure and temperature, which is of course not the case in a real SLB. Numerical results in Fig. 4 show that the temperature and pressure in the outer layer are in fact very high, of the order 10^4 K and 10^5 atm. However, taking this into consideration, the refractive index n_2 estimated will be larger than 1, and an even smaller enhancement is expected.

Our conclusion is therefore that the changes in the refractive indices due to compressional waves do not give rise to strong enhancement of the spontaneous decay rate inside a

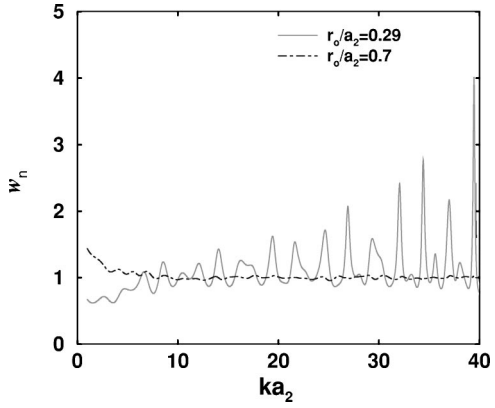

FIG. 6. Same as in Fig. 5; however, the value of n_1 is artifically increased to 1.5. The dipole is located at $r_0=0.29a_2$ and $0.7a_2$. The MDR peaks appear again due to the larger discontinuity in the refractive index at the boundary. However, after spectral averaging, the enhancement is again reduced to the order of 1.

SLB. This conclusion is robust against errors in the estimation of the refractive indices, since even if we artificially boost n_1 up to 1.5, so that the reflection at the boundary of the core and layer is strong enough to produce MDR's, as shown in Fig. 6, the enhancement is insignificant when we average over the frequency. Numerical simulations of hydrodynamics also suggest that during the collapsing phase of a SLB, a thin but dense shock fronts can emerge under certain circumstances [10–14,38]. Our shock wave model is similar to the compressional wave model, except that there is now one more layer outside the core. The radii and refractive indices of the core and the layers are a_i and n_i, respectively, where $i=1$, 2, and 3 starting from the core to the outer layers, and the ambient medium is water, with refractive index $n_4=1.33$. Once again, the refractive indices inside and outside the shock front are set to be 1.16 and 1, respectively. We have used the parameters $a_1/a_3=0.1$ and $a_2/a_3=0.12$ in our calculation to mimic the situation shown in Fig. 4(b). In other words, the thickness of the shock front is $0.02a_3$.

The spectrum of the normalized transition rates inside various layers of our shock SLB are shown in Fig. 7, which is similar to that of the compressional wave model and does not show any enhancement feature. Again, minor adjustments in the refractive indices do not affect the enhancement significantly.

In summary, the multilayered SLB configurations we have studied, which are motivated by numerical hydrodynamic results, only give a mild enhancement of the EM fields inside the bubble. However, so far we have ignored the effects of ionization on the refractive indices. When that is included, a strong effect is observed, as we shall discuss in Sec. VII.

VII. PLASMA SHELL MODEL

Under the high temperature and pressure inside a SLB, a fraction of the molecules (atoms) may be ionized and a thin plasma shell could be formed [11,14,15]. Other than the density of dipoles, the degree of ionization of atoms (molecules) is another factor that affects the refractive index. For most substances, especially stable elements such as argon, this is

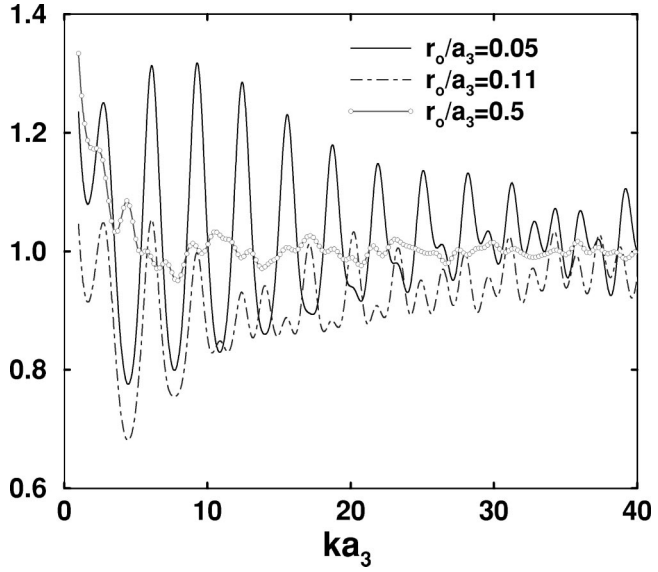

FIG. 7. Normalized emission rate of a dipole inside a gas bubble with shock waves, which has a small central core, a thin intermediate layer, and a thick outer shell, and is surrounded by water. The radius of the whole bubble is a_3, the radius of the core is $a_1=0.1a_3$ and the thickness of the thin shell is $a_2-a_1=0.02a_3$, where $a_2=0.12a_3$ is the outer radius of the intermediate shell. The solid line shows the normalized emission rate of a dipole in the central core at $r_0=0.05a_3$. The dashed line represents that of dipole in the intermediately layer at $r_0=0.11a_3$, and the circled line shows the corresponding value in the outer layer at $r_0=0.5a_3$. In all the situations, no enhancement is observed.

usually ignored under ordinary conditions. However, when taken into account, as needed for the extraordinary conditions inside a SLB, we will show that this effect is by no means negligible, especially inside the shock front.

The dielectric constant in the plasma shell is given by [35]

$$\epsilon(\omega)=\epsilon_0-\frac{\omega_p^2}{\omega^2}, \tag{7.1}$$

where ω_p is the plasma frequency defined by

$$\omega_p^2=\frac{4\pi N_e e^2}{m_e}. \tag{7.2}$$

Here $\epsilon_0=1.16$, and N_e is the number density of free electrons in the plasma, which can be estimated by the Saha equations [28,39]

$$\frac{N_e^2}{N_{Ar}}=2\left(\frac{2\pi m_e k}{h^2}\right)^{3/2}T^{3/2}e^{-I/kT}, \tag{7.3}$$

where N_{Ar}, I, and T are the number density of argon, the ionization energy of argon atoms, and the temperature of the shock front, respectively. Regarding the consistency with numerical and experimental results obtained so far [10–13,38], we have assumed that the SLB consists of pure argon, with the same mass density as that of water and temperature 5×10^4 K inside the shock. It is also assumed that higher ionizations of argon are negligible; hence, $I=15.755$ eV, the first ionization energy of argon [40]. Our calculation

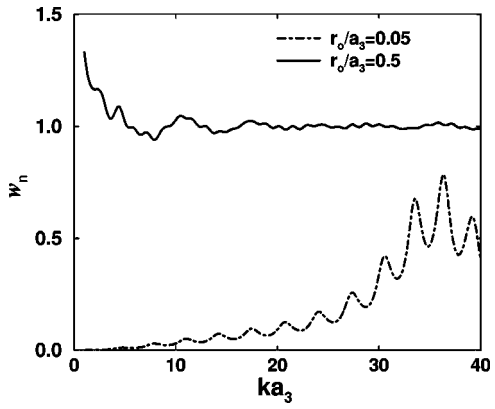

FIG. 8. Normalized emission rate of a dipole inside a gas bubble where a plasma shell has been developed. The refractive index of the plasma shell is taken to be 0.01, and its radius is $0.1a_3$. Except for the plasma shell, the model is exactly the same as that shown in Fig. 7. The normalized emission rate for a dipole inside the core at $r_0=0.05a_3$ and in the outer layer at $r_0=0.5a_3$ are shown, respectively, by the dashed and solid lines, with neither of them showing significant enhancement.

gives a $\sim$30% ionization, which shows that the plasma is not weakly ionized. From Eq. (7.2), it is found that the plasma frequencies fall inside the optical frequency range for typical values of density and temperature in a SLB, which implies that the refractive index could be very small in the shock-front. Hereafter, the value of the refractive index of this plasma shell will be set to be 0.01 for simplicity, unless otherwise specified.

In Fig. 8 we show the normalized transition rate versus frequency for a dipole inside the core and the outermost layer, and there is no enhancement in these regions. conversely, an enhancement of $\sim$20–30 in the optical range is observed inside the shell, as shown in Fig. 9. We conjecture that the enhanced radiation by the atoms inside the plasma shell is the origin of SL. This enhancement is due to the contribution of the longitudinal part of the fields, which is discontinuous across the gas-plasma boundary, with a jump of 10^4 if $n_2=0.01$. Contrary to MDR, which is a resonance effect, this enlargement of the electric field is independent of

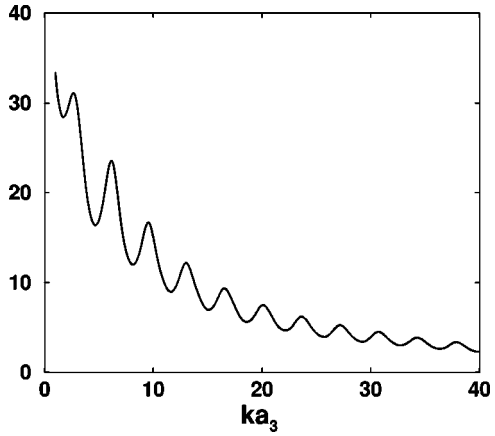

FIG. 9. Same as in Fig. 8; however, the normalized emission rate for a dipole inside the plasma shell is shown. Inside the plasma shell, significant enhancement is observed, contrary to the situations depicted in Fig. 8.

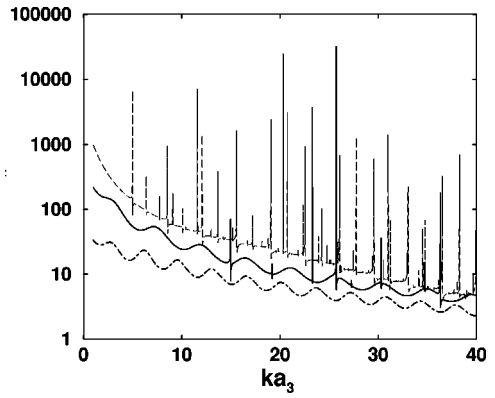

FIG. 10. Normalized emission rate of a dipole inside the plasma shell developed in a gas bubble. The thickness of the shell is $0.02a_3$, while its inner radius is $0.1a_3$ (dash-dotted line), $0.3a_3$ (solid line), and $0.9a_3$ (dashed line), where a_3 is the radius of the bubble. It can be observed that the emission rate increases with the distance of the shell from the center.

the frequency and hence gives rise to a uniform background which can survive the frequency averaging.

A further investigation shows that the transition rate inside the shell may depend on several parameters in addition to the refractive indices. These include the thickness of the shell and its distance from the center, etc. In Fig. 10 we compare the spectra at the center of plasma shells with the same thickness, but situated in different locations in a SLB. We conclude that there is stronger enhancement when the shell is farther from the center. Because the size of the SLB is comparable to optical wavelengths, this represents the coincidence of the shell with the first peak of the field near the boundary.

We also observe that the transition rate inside the shell is very sensitive to the thickness of the shell. Figure 11 shows the spectra at the centers of shells with various thicknesses located at a distance $0.1a_3$ from the bubble center. The patterns of the spectral lines are very similar, but their amplitudes are magnified by a factor $\sim$5 when the shell thicknesses are halved.

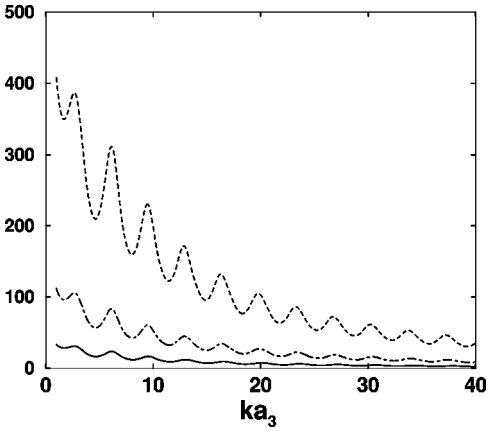

FIG. 11. Normalized emission rate of a dipole inside the plasma shell developed in a gas bubble. The distance of the shell from the center is $0.1a_3$, while its thickness is $0.02a_3$ (solid line), $0.01a_3$ (dash-dotted line), and $0.005a_3$ (dashed line), where a_3 is the radius of the SLB. It is observed that the emission rate increases drastically with thinner shells.

VIII. SUMMARY

To summarize, in this paper we proposed a model of SLB as a multilayered dielectric sphere with a plasma shell. Our model is based on the strong evidences of the existence of shock waves inside a SLB. We showed that while homogeneous spheres and layered spheres with compressional waves give insignificant enhancement to light emission in SLB's, an enhancement factor in the spontaneous emission rate of order 100 can be achieved for atoms located inside a narrow plasma layer where the dielectric constant is small. We conjecture that this represents approximately the configuration in a SLB when it is compressed to its minimum radius, characterized by the presence of plasma within a thin shell surrounding the core of the bubble. With this enhancement, the atoms inside the shell radiate with a shorter lifetime compared to that in vacuum, and this effect may explain the narrowness of SL pulses [21]. The spatially averaged enhancement depends on the location of the shell, as well as its thickness. Generally speaking, the enhacement increases with the distance from the shell to the core, and decreases with its thickness. We also estimate the degree of ionization required to give this enhancement and the corresponding temperature, by using the Saha equation [28,39]. We find that a strong degree of ionization $\sim 30\%$ is required, which is possible in a SLB at temperature $\sim 5\times 10^4$ K. This value is inside the typical range of numerical and experimental data obtained so far.

It is worth noticing that at higher temperatures, and therefore stronger ionizations, the refractive index in the shell will become negative, which means the shell is strongly absorptive and dispersive. This interesting topic, namely, quantum optics in absorptive and dispersive media, is still open for exploration [41–43]. Though we have not considered it rigorously in this paper, detailed studies on the quautum behavior of this absorptive system, are in progress, and the result will be reported elsewhere.

The enhancement effect considered in the present paper is a final state effect. That is, it affects radiative rates via the photon phase space factor. In addition to enhancing the spontaneous emission rate, it could influence other radiative processes as well. For example, in a recently proposed SL model that considered how the blackbody radiation spectrum could be modified by the photon-absorption processes [28], both the emission and absorption mechanisms proved likely to be affected by the formation of a plasma shell in a SLB. In addition, other de-excitation processes, such as radiative recombination, radiative electronic transitions, radiative rotational or vibrational transitions, bremsstrahlung, or even collision-induced emission, which have been invoked to interpret the phenomenon of SL [29], are also dependent on the phase space structure of the emitted photons. The major goal of our paper is primarily to show that the extreme physical conditions achievable in a SLB, namely, high density, high temperature, ionization, and finite size could indeed affect various light emission processes. At the first stage of an exhaustive investigation, in the present paper we studied their influences on the process of spontaneous emission, and showed that an enhancement factor of about 10–100 in the spontaneous decay rate is achievable in the presence of a thin plasma shell. To compute the emission spectrum of a SLB, one has to consider all these factors, incorporating numerical fluid dynamics, plasma formation and radiation processes. We are currently working along this direction, and relevant results will be reported in due course.

ACKNOWLEDGMENTS

This research was partially supported by RGC Earmarked Grant No. CUHK312/96P and a Direct Grant (Grant No. 2060093) from the Chinese University of Hong Kong. P.T.L.'s work was also supported by RGC Earmarked Grant No. CUHK4282/00P. We acknowledge the computer science center of the Chinese University of Hong Kong for providing computer time at the CUHK Origin 2000.

[1] H. Frenzel and H. Schultes, Z. Phys. Chem. Abt. B **27**, 421 (1934).
[2] B.P. Barber, R.A. Hiller, R. Löfstedt, S.J. Putterman, and K.R. Weninger, Phys. Rep. **281**, 65 (1997).
[3] D.F. Gaitan, Ph.D. thesis, University of Mississippi, 1990.
[4] D.F. Gaitan and L.A. Crum, *Proceedings of the 12th International Symposium on Nonlinear Acoustics* (Elsevier, New York, 1991).
[5] B.P. Barber and S.J. Putterman, Nature (London) **352**, 318 (1991).
[6] D.F. Gaitan, L.A. Crum, C.C. Church, and R.A. Roy, J. Acoust. Soc. Am. **91**, 3166 (1992).
[7] L.A. Crum and S. Cordry, in *Proceedings of IUTAM Symposium on Bubble Dynamics and Interface Phenomena*, edited by J.R. Blake and N.H. Thomas (Kluwer, Dordrecht, 1994).
[8] K.S. Suslick, T. Hyeon, M. Fang, J.T. Ries, and A.A. Cichowlas, Mater. Sci. Forum **225**, 903 (1996).
[9] P. Jarman, J. Acoust. Soc. Am. **32**, 1459 (1960).
[10] C.C. Wu and P.H. Roberts, Phys. Rev. Lett. **70**, 3424 (1993).
[11] W.C. Moss, D.B. Clarke, J.W. White, and D.A. Young, Phys. Fluids **6**, 2979 (1994).
[12] H.Y. Cheng, M.-C. Chu, P.T. Leung, and L. Yuan, Phys. Rev. E **58**, R2705 (1998).
[13] L. Yuan, H.Y. Cheng, M.-C. Chu, and P.T. Leung, Phys. Rev. E **57**, 4265 (1998).
[14] W. Moss, D.B. Clarke, and D.A. Young, Science **276**, 1398 (1997).
[15] Ning Xu, Long Wang, and Xiwei Hu, Phys. Rev. E **57**, 1615 (1998); Phys. Rev. Lett. **83**, 2441 (1999).
[16] M.P. Brenner, D. Lohse, D. Oxtoby, and T.F. Dupont, Phys. Rev. Lett. **76**, 1158 (1996).
[17] J.R. Willison, Phys. Rev. Lett. **81**, 5430 (1998).
[18] B.P. Barber, R. Hiller, K. Arisaka, H. Fetterman, and S.J. Putterman, J. Acoust. Soc. Am. **91**, 3061 (1992).
[19] B.P. Barber and S.J. Putterman, Phys. Rev. Lett. **69**, 3839 (1992).
[20] R.A. Hiller, S.J. Putterman, and B.P. Barber, Phys. Rev. Lett. **69**, 1182 (1992).
[21] B.P. Barber, C.C. Wu, R. Löfstedt, P.H. Roberts, and S.J. Putterman, Phys. Rev. Lett. **72**, 1380 (1994).
[22] R.A. Hiller, K. Weninger, S.J. Putterman, and B.P. Barber, Science **266**, 248 (1994).

[23] B.P. Barber, K. Weninger, R. Löfstedt, and S. Putterman, Phys. Rev. Lett. **74**, 5276 (1995).
[24] K.R. Weninger, B.P. Barber, and S.J. Putterman, Phys. Rev. E **54**, R2205 (1996).
[25] K.R. Weninger, B.P. Barber, and S.J. Putterman, Phys. Rev. Lett. **78**, 1799 (1997).
[26] R.A. Hiller, S.J. Putterman, and K.R. Weninger, Phys. Rev. Lett. **80**, 1090 (1998).
[27] B. Gompf, R. Günther, G. Nick, R. Pecha, and W. Eisenmenger, Phys. Rev. Lett. **79**, 1405 (1997).
[28] S. Hilgenfeldt, S. Grossmann, and D. Lohse, Nature (London) **398**, 402 (1999); Phys. Fluids **11**, 1318 (1999).
[29] L. Frommhold, Phys. Rev. E **58**, 1899 (1998).
[30] C. Eberlein, Phys. Rev. A **53**, 2772 (1996); Phys. Rev. Lett. **76**, 3842 (1996).
[31] E.M. Purcell, Phys. Rev. **69**, 681 (1946).
[32] S.C. Ching, H.M. Lai, and K. Young, J. Opt. Soc. Am. B **4**, 1995 (1987).
[33] H.M. Lai, P.T. Leung, and K. Young, Phys. Rev. A **37**, 1597 (1988).
[34] A.J. Campillo, J.D. Eversole and H.-B. Lin, in *Optical Processes in Microcavities*, edited by R.K. Chang and A.J. Campillo (World Scientific, Singapore, 1996), and references therein.
[35] J.D. Jackson, *Classical Electrodynamics* (Wiley, New York, 1975).
[36] L. Mandel and E. Wolf, *Optical Coherence and Quantum Optics* (Cambridge, New York, 1995).
[37] E.S.C. Ching, P.T. Leung, and K. Young, in *Optical Processes in Microcavities*, (Ref. [34]), and references therein.
[38] M.-C. Chu and D. Leung, J. Phys.: Condens. Matter **9**, 3387 (1997).
[39] Y.B. Zel'dovich and Y.P. Raizer, *Physics of Shock Waves and High-Temperature Hydrodynamic Phenomena* (Academic, New York, 1966).
[40] C.Y. Ho, L. Yuan, M.-C. Chu, P.T. Leung, and W. Wei (unpublished).
[41] R. Matloob, R. Loudon, S.M. Barneet, and J. Jeffers, Phys. Rev. A **52**, 4823 (1995).
[42] R. Matloob and R. Loudon, Phys. Rev. A **53**, 4567 (1996).
[43] S.M. Barnett, B. Huttner, R. Loudon, and R. Matloob, J. Phys. B **29**, 3763 (1996).